Damjan Banić
Goran Turkalj
Josip Brnić

DOI: 10.21278/TOF.40206
ISSN 1333-1124
eISSN 1849-1391

FINITE ELEMENT STRESS ANALYSIS OF ELASTIC BEAMS UNDER NON-UNIFORM TORSION

Summary

This paper presents a two-dimensional finite element formulation for the stress analysis of elastic beams subjected to non-uniform torsion. The element stiffness matrix and load vectors are derived using the primary and secondary warping functions. The primary function corresponds to that occurring with uniform torsion problems. The secondary function is introduced to take into account effects caused by the restrained warping. Thus, shear stresses are divided into the primary and secondary ones, keeping the same meaning as the warping functions. The proposed finite element model enables the stress analysis to be carried out regardless of cross-sectional shapes. The material is assumed to obey Hooke's law. The effectiveness of the presented finite element algorithm is validated through two benchmark examples.

Key words: *non-uniform torsion, warping function, shear stress, finite elements*

1. Introduction

Basic torsion theory, referred to as St. Venant's or uniform torsion theory, is well described in literature [1-4] and has been, for a long time, a fundamental theory applied by many researchers in the field of torsion. If the warping effects are to be taken into account, the non-uniform torsion theory has to be applied [5, 6]. The development of the computational science and of numerical analysis resulted in numerous methods, e.g. finite element method, finite difference method, finite volume method, etc. Merging torsion theories with numerical analysis opens up new possibilities in predicting and modelling various types of structures and machine elements submitted to a torsion type of load. Some numerical solutions to the uniform torsion problem are presented in Refs. 1, 7 and 8, while those used in the non-uniform torsion problem solving are given in Refs. 9-16.

In modern engineering practice, engineers seeking practical solutions often tend to idealize their input parameters. Such a procedure often gives good approximate results although it does not give a real insight into the behaviour of the structural member discussed. When talking about torsion, these idealizations usually prefer to neglect the effects of restrained warping, which always occur when beams have particular restraints. Although, the fact is that in the long beams or in the beams having low torsional and high sectoral rigidities such effects are usually negligible. Therefore, some authors, to simplify their analyses, refer to three types of cross-sections: solid, closed thin-walled and open thin-walled sections and they point out the open thin-walled sections when dealing with restrained warping [1].

This paper presents a finite element formulation for the linear stress analysis of beams subjected to non-uniform torsion. The applied torsion theory is a modified theory originally presented by Sapountzakis [9]. The described numerical model uses an isoparametric quadrilateral nine-node element presented by Pilkey [1]. The element stiffness matrix and load vectors are derived using the primary and secondary warping functions. The primary warping function corresponds to that occurring with uniform torsion problems. The secondary warping function is introduced to account for the shear stress due to restrained warping effects. Thus, the shear stress is divided into the primary and the secondary one, where the former appears due to uniform torsion and the latter due to restrained warping. The proposed finite element model enables the stress analysis to be carried out regardless of cross-sectional shapes. The material is assumed to obey Hooke's law. The computer program is written using the Python programming language. The effectiveness of the algorithm discussed is validated through two benchmark examples.

2. Basic considerations

A right-handed Cartesian coordinate system (x, y, z) is chosen in such a way that the z-axis coincides with the beam axis passing through the centroid of each cross-section. The shear centre of the cross-section is defined by the position coordinates x_S and y_S. The displacement field is taken as

$$\begin{aligned} u(y,z) &= -(y-y_S)\varphi(z), \quad v(x,z) = (x-x_S)\varphi(z) \\ w(x,y,z) &= \varphi'(z)\omega_I(x,y) - 2(1+\nu)\varphi'''(z)\omega_{II}(x,y) \end{aligned} \tag{1}$$

where u, v and w are the rigid-body translations of the cross-section in the x-, y- and z-directions, respectively; φ is the angle of twist about the shear centre; ν is Poisson's ratio; ω_I and ω_{II} are the primary and secondary warping functions, respectively. The secondary warping function is introduced to obtain the secondary shear stress due to restrained warping [9]. The non-zero strain components are found from the first order strain-displacement relations as

$$\varepsilon_z = \frac{\partial w}{\partial z} = \varphi''\omega_I - 2(1+\nu)\varphi''''\omega_{II}, \tag{2}$$

and

$$\begin{aligned} \gamma_{zx} &= \frac{\partial u}{\partial z} + \frac{\partial w}{\partial x} = \varphi'\left(\frac{\partial \omega_I}{\partial x} - y + y_S\right) - 2(1+\nu)\varphi''\frac{\partial \omega_{II}}{\partial x} \\ \gamma_{zy} &= \frac{\partial v}{\partial z} + \frac{\partial w}{\partial y} = \varphi'\left(\frac{\partial \omega_I}{\partial y} + x - x_S\right) - 2(1+\nu)\varphi''\frac{\partial \omega_{II}}{\partial y} \end{aligned} \tag{3}$$

If the fourth order derivative of the angle of twist is left out from Eq. (2), stress components of a linear elastic material are calculated as

$$\begin{aligned} \sigma_z &= E\varepsilon_z = E\varphi''\omega_I \\ \tau_{zx} &= G\gamma_{zx} = G\varphi'\left(\frac{\partial \omega_I}{\partial x} - y + y_S\right) - E\varphi''\frac{\partial \omega_{II}}{\partial x} \\ \tau_{zy} &= G\gamma_{zy} = G\varphi'\left(\frac{\partial \omega_I}{\partial y} + x - x_S\right) - E\varphi''\frac{\partial \omega_{II}}{\partial y} \end{aligned} \tag{4}$$

The shear stress is decomposed into a primary and a secondary part due to the uniform and the non-uniform torsion, respectively, i.e.

$$\tau_{zx} = \tau_{zx}^{\mathrm{sv}} + \tau_{zx}^{\omega}, \quad \tau_{zy} = \tau_{zy}^{\mathrm{sv}} + \tau_{zy}^{\omega}$$
$$\tau_{zx}^{\mathrm{sv}} = G\varphi'\left(\frac{\partial \omega_{\mathrm{I}}}{\partial x} - y + y_{\mathrm{S}}\right), \quad \tau_{zy}^{\mathrm{sv}} = G\varphi'\left(\frac{\partial \omega_{\mathrm{I}}}{\partial y} + x - x_{\mathrm{S}}\right) \tag{5}$$
$$\tau_{zx}^{\omega} = -E\varphi'''\frac{\partial \omega_{\mathrm{II}}}{\partial x}, \quad \tau_{zy}^{\omega} = -E\varphi'''\frac{\partial \omega_{\mathrm{II}}}{\partial y}$$

From Eq. (4), equilibrium equations form the following expressions:

$$\frac{\partial \tau_{zx}}{\partial z} = G\varphi''\left(\frac{\partial \omega_{\mathrm{I}}}{\partial x} - y + y_{\mathrm{S}}\right) - E\varphi''''\frac{\partial \omega_{\mathrm{II}}}{\partial x} = 0$$
$$\frac{\partial \tau_{zy}}{\partial z} = G\varphi''\left(\frac{\partial \omega_{\mathrm{I}}}{\partial y} + x - x_{\mathrm{S}}\right) - E\varphi''''\frac{\partial \omega_{\mathrm{II}}}{\partial y} = 0 \tag{6}$$

and

$$\frac{\partial \tau_{zx}}{\partial x} + \frac{\partial \tau_{zy}}{\partial y} + \frac{\partial \sigma_z}{\partial z} = G\varphi'\left(\frac{\partial^2 \omega_{\mathrm{I}}}{\partial x^2} + \frac{\partial^2 \omega_{\mathrm{I}}}{\partial y^2}\right) - E\varphi'''\left(\frac{\partial^2 \omega_{\mathrm{II}}}{\partial x^2} + \frac{\partial^2 \omega_{\mathrm{II}}}{\partial y^2}\right) + E\varphi'''\,\omega_{\mathrm{I}} = 0. \tag{7}$$

Furthermore, Eq. (7) is decomposed into two partial differential equations:

$$\nabla^2 \omega_{\mathrm{I}} = \frac{\partial^2 \omega_{\mathrm{I}}}{\partial x^2} + \frac{\partial^2 \omega_{\mathrm{I}}}{\partial y^2} = 0, \tag{8}$$

$$\nabla^2 \omega_{\mathrm{II}} = \frac{\partial^2 \omega_{\mathrm{II}}}{\partial x^2} + \frac{\partial^2 \omega_{\mathrm{II}}}{\partial y^2} = \omega_{\mathrm{I}}. \tag{9}$$

It can be observed that both warping functions, ω_{I} and ω_{II}, are modelled by Eqs. (8) and (9). Boundary conditions for partial differential equations (8) and (9) are, respectively,

$$\tau_{zx}^{\mathrm{sv}} n_x + \tau_{zy}^{\mathrm{sv}} n_y = 0, \tag{10}$$

$$\tau_{zx}^{\omega} n_x + \tau_{zy}^{\omega} n_y = 0. \tag{11}$$

The warping functions, defined in Eqs. (8) and (9), are calculated with respect to the shear centre. Stress resultants acting on each cross-section of the beam can be defined as follows:

$$B_{\omega} = \int_A \sigma_z \omega_{\mathrm{I}}\, dA = E\varphi'' \int_A \omega_{\mathrm{I}}^2\, dA = EI_{\omega}\varphi'', \quad I_{\omega} = \int_{\Omega} \omega_{\mathrm{I}}^2\, dA, \tag{12}$$

$$M_z = \int_A \left[\tau_{zy}(x - x_{\mathrm{S}}) - \tau_{zx}(y - y_{\mathrm{S}})\right] dA = T_{\mathrm{sv}} + T_{\omega}, \tag{13}$$

where B_{ω} is the bimoment, while I_{ω} represents the warping moment of inertia. The torsional moment M_z consists of two parts: T_{sv} and T_{ω}, representing St. Venant's or the uniform torsion moment and the warping or the non-uniform torsion moment, respectively. From Eqs. (5) and (13), the components of torsional moment can be expressed as

$$T_{\mathrm{sv}} = \int_A \left[\tau_{zy}^{\mathrm{sv}}(x - x_{\mathrm{S}}) - \tau_{zx}^{\mathrm{sv}}(y - y_{\mathrm{S}})\right] dA = GI_{\mathrm{t}}\varphi'$$
$$I_{\mathrm{t}} = \int_A \left[(x - x_{\mathrm{S}})^2 + (y - y_{\mathrm{S}})^2 + (x - x_{\mathrm{S}})\frac{\partial \omega_{\mathrm{I}}}{\partial y} - (y - y_{\mathrm{S}})\frac{\partial \omega_{\mathrm{I}}}{\partial x}\right] dA \tag{14}$$

and

$$T_{\omega} = \int_A \left[\tau_{zy}^{\omega}(x - x_{\mathrm{S}}) - \tau_{zx}^{\omega}(y - y_{\mathrm{S}})\right] dA = -EI_{\mathrm{II}}\varphi'''$$
$$I_{\mathrm{II}} = \int_A \left[(x - x_{\mathrm{S}})\frac{\partial \omega_{\mathrm{II}}}{\partial y} - (y - y_{\mathrm{S}})\frac{\partial \omega_{\mathrm{II}}}{\partial x}\right] dA \tag{15}$$

In Eq. (14), I_t denotes the St. Venant torsional constant, while I_{II} from Eq. (15) represents the warping moment of inertia due to the secondary warping function analogous to I_ω. The differential equation for the non-uniform torsion follows from the inclusion of Eqs. (14) and (15) into Eq. (13)

$$M_z = -EI_{II}\,\varphi''' + GI_t\,\varphi', \tag{16}$$

and if expressed in terms of the continuous torsional moment m_z

$$m_z = EI_{II}\,\varphi'''' - GI_t\,\varphi'', \quad m_z = -\frac{dM_z}{dz}. \tag{17}$$

By solving the differential equation from Eq. (16) or (17), the expression for the angle of twist is derived. The analytical solution to Eq. (17) is taken from Chen and Atsuta [3], as

$$\varphi(z) = C_1 + C_2\,z + C_3\cosh(\alpha z) + C_4\sinh(\alpha z) - \frac{m_z z^2}{2GI_t}, \quad \alpha = \sqrt{\frac{GI_t}{EI_{II}}}. \tag{18}$$

3. Finite element formulation

In the stress analysis procedure, the first step is the calculation of the primary and secondary warping functions, followed by the determination of the torsional constant and the warping moment of inertia. Once obtained, these values are used for the calculation of the angle of twist, from Eq. (18), and, lastly, of the stresses from Eqs. (4) and (5).

To calculate the warping functions, the procedure continues with the discretization of the cross-section with finite elements. Isoparametric quadrilateral nine-node elements are used, where the Lagrangian shape functions are:

$$\begin{aligned}
&\mathbf{N}(\eta,\zeta) = \frac{1}{4}\begin{bmatrix} N_1 & N_2 & N_3 & N_4 & N_5 & N_6 & N_7 & N_8 & N_9 \end{bmatrix}\\
&N_1(\eta,\zeta) = \eta\zeta(1-\eta)(1-\zeta), \quad N_2(\eta,\zeta) = -2\eta(1-\eta)(1-\zeta^2)\\
&N_3(\eta,\zeta) = -\eta\zeta(1-\eta)(1+\zeta), \quad N_4(\eta,\zeta) = -2\zeta(1-\eta^2)(1-\zeta)\\
&N_5(\eta,\zeta) = 4(1-\eta^2)(1-\zeta^2), \quad N_6(\eta,\zeta) = 2\zeta(1-\eta^2)(1+\zeta)\\
&N_7(\eta,\zeta) = -\eta\zeta(1+\eta)(1-\zeta), \quad N_8(\eta,\zeta) = 2\eta(1+\eta)(1-\zeta^2)\\
&N_9(\eta,\zeta) = \eta\zeta(1+\eta)(1+\zeta)
\end{aligned} \tag{19}$$

The warping functions are calculated by solving the partial differential equations from Eqs. (8) and (9) with the boundary conditions from Eqs. (10) and (11). After applying the weighted residual method to Eq. (8), it follows that

$$\begin{aligned}
&\int_A r\nabla^2\omega_I\,dA + \oint_s \bar{r}\,(\mathbf{n}\cdot\mathbf{g} - \mathbf{n}\cdot\nabla\omega_I)\,ds = 0\\
&\nabla = \mathbf{i}\frac{\partial}{\partial x} + \mathbf{j}\frac{\partial}{\partial y}, \quad \mathbf{n} = n_x\,\mathbf{i} + n_y\,\mathbf{j}, \quad \mathbf{g} = (y - y_S)\mathbf{i} - (x - x_S)\mathbf{j}
\end{aligned} \tag{20}$$

where the second integral in Eq. (20) implies the boundary condition in vector notation. The integral form in Eq. (20) is referred to as a "weak formulation". If the test functions r and $\bar{r}$ are chosen to be identical and if Green's first identity and the divergence theorem are used, the weak formulation takes the final form

$$\int_A \nabla r\cdot\nabla\omega_I\,dA - \int_A \mathbf{g}\cdot\nabla r\,dA = 0. \tag{21}$$

Now, if the finite element form is applied by the inclusion of

$$\omega_I(\eta,\zeta) = \mathbf{N}(\eta,\zeta)\,\boldsymbol{\omega}_I^e, \quad r = \mathbf{N}(\eta,\zeta)\,\mathbf{r}^e = \mathbf{r}^{e^T}\mathbf{N}^T, \tag{22}$$

the following expression is obtained:

$$\int_A \mathbf{r}^{\mathrm{e}\mathrm{T}}\left[\left(\nabla\mathbf{N}^{\mathrm{T}}\cdot\nabla\mathbf{N}\right)\boldsymbol{\omega}_{\mathrm{I}}^{\mathrm{e}}-\nabla\mathbf{N}^{\mathrm{T}}\cdot\mathbf{g}^{\mathrm{T}}\right]dA=0. \tag{23}$$

And for each element, there is a form

$$\mathbf{r}^{\mathrm{e}\mathrm{T}}\left(\mathbf{k}^{\mathrm{e}}\boldsymbol{\omega}^{\mathrm{e}}-\mathbf{p}^{\mathrm{e}}\right)=0,\quad \mathbf{k}^{\mathrm{e}}\boldsymbol{\omega}^{\mathrm{e}}=\mathbf{p}^{\mathrm{e}}. \tag{24}$$

The solution to the primary warping function is obtained by solving Eq. (23) for each element. The weak formulation for the second partial differential equation, Eq. (9), is taken as

$$\begin{aligned}&\int_A r\left[\nabla^2\omega_{\mathrm{II}}-\omega_{\mathrm{I}}\right]dA-\oint_s \bar{r}\,\mathbf{n}\cdot\nabla\omega_{\mathrm{II}}\,ds=0\\&\nabla=\mathbf{i}\frac{\partial}{\partial x}+\mathbf{j}\frac{\partial}{\partial y},\quad \mathbf{n}=n_x\,\mathbf{i}+n_y\,\mathbf{j}\end{aligned} \tag{25}$$

Once again, if the test functions r and $\bar{r}$ are chosen to be identical and Green's first identity and the divergence theorem are used, the weak formulation takes the final form

$$\int_A\left[-\nabla r\cdot\nabla\omega_{\mathrm{II}}-r\,\omega_{\mathrm{I}}\right]dA=0. \tag{26}$$

The finite element form is applied by the inclusion of

$$\omega_{\mathrm{II}}(\eta,\zeta)=\mathbf{N}(\eta,\zeta)\boldsymbol{\omega}_{\mathrm{II}}^{\mathrm{e}},\quad \omega_{\mathrm{I}}(\eta,\zeta)=\mathbf{N}(\eta,\zeta)\boldsymbol{\omega}_{\mathrm{I}}^{\mathrm{e}},\quad r=\mathbf{N}(\eta,\zeta)\mathbf{r}^{\mathrm{e}}=\mathbf{r}^{\mathrm{e}\mathrm{T}}\mathbf{N}^{\mathrm{T}}, \tag{27}$$

and it is obtained that

$$\int_A \mathbf{r}^{\mathrm{e}\mathrm{T}}\left[\left(\nabla\mathbf{N}^{\mathrm{T}}\cdot\nabla\mathbf{N}\right)\boldsymbol{\omega}_{\mathrm{II}}^{\mathrm{e}}+\left(\mathbf{N}^{\mathrm{T}}\cdot\mathbf{N}\right)\boldsymbol{\omega}_{\mathrm{I}}^{\mathrm{e}}\right]dA=0. \tag{28}$$

The solution to the second warping function is obtained by solving Eq. (28) for each element. The stiffness matrix is of the same form for both partial differential equations, and it is calculated as

$$\mathbf{k}^{\mathrm{e}}=\iint_A\left(\nabla\mathbf{N}^{\mathrm{T}}\cdot\nabla\mathbf{N}\right)dxdy=\iint_A\left(\frac{\partial\mathbf{N}^{\mathrm{T}}}{\partial x}\frac{\partial\mathbf{N}}{\partial x}+\frac{\partial\mathbf{N}^{\mathrm{T}}}{\partial y}\frac{\partial\mathbf{N}}{\partial y}\right)dxdy. \tag{29}$$

To make the transformation from the real domain (x, y) to the reference domain (η, ζ), first, the Jacobian matrix has to be calculated

$$\mathbf{J}=\begin{bmatrix}\dfrac{\partial x}{\partial\eta} & \dfrac{\partial y}{\partial\eta}\\ \dfrac{\partial x}{\partial\zeta} & \dfrac{\partial y}{\partial\zeta}\end{bmatrix}=\begin{bmatrix}\dfrac{\partial\mathbf{N}}{\partial\eta}\mathbf{x} & \dfrac{\partial\mathbf{N}}{\partial\eta}\mathbf{y}\\ \dfrac{\partial\mathbf{N}}{\partial\zeta}\mathbf{x} & \dfrac{\partial\mathbf{N}}{\partial\zeta}\mathbf{y}\end{bmatrix}=\begin{bmatrix}\dfrac{\partial\mathbf{N}}{\partial\eta}\\ \dfrac{\partial\mathbf{N}}{\partial\zeta}\end{bmatrix}\begin{bmatrix}\mathbf{x} & \mathbf{y}\end{bmatrix}. \tag{30}$$

If transforming the integral, one has to add the determinant of the Jacobian matrix, or the "Jacobian" under the integral. For example, if transforming the expression for the surface of the element from the real domain Ω to the reference domain Ω_{r}, it is calculated as

$$A_{\mathrm{e}}=\int_\Omega dxdy=\int_{\Omega_{\mathrm{r}}}\left|\mathbf{J}_{\mathrm{e}}\right|d\eta d\zeta. \tag{31}$$

The gradient of the shape function matrix $\nabla\mathbf{N}$ is calculated as

$$\nabla\mathbf{N}=\begin{bmatrix}\dfrac{\partial\mathbf{N}}{\partial x}\\ \dfrac{\partial\mathbf{N}}{\partial y}\end{bmatrix}=\begin{bmatrix}\dfrac{\partial\mathbf{N}}{\partial\eta}\dfrac{\partial\eta}{\partial x}+\dfrac{\partial\mathbf{N}}{\partial\zeta}\dfrac{\partial\zeta}{\partial x}\\ \dfrac{\partial\mathbf{N}}{\partial\eta}\dfrac{\partial\eta}{\partial y}+\dfrac{\partial\mathbf{N}}{\partial\zeta}\dfrac{\partial\zeta}{\partial y}\end{bmatrix}=\begin{bmatrix}\dfrac{\partial\eta}{\partial x} & \dfrac{\partial\zeta}{\partial x}\\ \dfrac{\partial\eta}{\partial y} & \dfrac{\partial\zeta}{\partial y}\end{bmatrix}\begin{bmatrix}\dfrac{\partial\mathbf{N}}{\partial\eta}\\ \dfrac{\partial\mathbf{N}}{\partial\zeta}\end{bmatrix}=\mathbf{J}_{\mathrm{e}}^{-1}\begin{bmatrix}\dfrac{\partial\mathbf{N}}{\partial\eta}\\ \dfrac{\partial\mathbf{N}}{\partial\zeta}\end{bmatrix}=\mathbf{B}_{\mathrm{e}}=\mathbf{B}, \tag{32}$$

And, if transposed, then

$$\nabla \mathbf{N}^{\mathrm{T}} = \begin{bmatrix} \dfrac{\partial \mathbf{N}^{\mathrm{T}}}{\partial x} & \dfrac{\partial \mathbf{N}^{\mathrm{T}}}{\partial y} \end{bmatrix} = \begin{bmatrix} \dfrac{\partial \mathbf{N}^{\mathrm{T}}}{\partial \eta} & \dfrac{\partial \mathbf{N}^{\mathrm{T}}}{\partial \zeta} \end{bmatrix} \begin{bmatrix} \dfrac{\partial \eta}{\partial x} & \dfrac{\partial \eta}{\partial y} \\ \dfrac{\partial \zeta}{\partial x} & \dfrac{\partial \zeta}{\partial y} \end{bmatrix} = \begin{bmatrix} \dfrac{\partial \mathbf{N}^{\mathrm{T}}}{\partial \eta} & \dfrac{\partial \mathbf{N}^{\mathrm{T}}}{\partial \zeta} \end{bmatrix} \mathbf{J}_{\mathrm{e}}^{-1\mathrm{T}} = \mathbf{B}^{\mathrm{T}} . \tag{33}$$

If Eqs. (31), (32) and (33) are included into Eq. (29), the final expression for the stiffness matrix is derived as

$$\mathbf{k}^{\mathrm{e}} = \int_{-1}^{1}\int_{-1}^{1} \begin{bmatrix} \dfrac{\partial \mathbf{N}^{\mathrm{T}}}{\partial \eta} & \dfrac{\partial \mathbf{N}^{\mathrm{T}}}{\partial \zeta} \end{bmatrix} \mathbf{J}_{\mathrm{e}}^{-1\mathrm{T}} \mathbf{J}_{\mathrm{e}}^{-1} \begin{bmatrix} \dfrac{\partial \mathbf{N}}{\partial \eta} \\ \dfrac{\partial \mathbf{N}}{\partial \zeta} \end{bmatrix} |\mathbf{J}_{\mathrm{e}}| \, d\eta d\zeta = \int_{-1}^{1}\int_{-1}^{1} \mathbf{B}^{\mathrm{T}} \mathbf{B} |\mathbf{J}_{\mathrm{e}}| \, d\eta d\zeta . \tag{34}$$

The load vector which corresponds to Eq. (8) is

$$\mathbf{p}_{\mathrm{I}}^{\mathrm{e}} = \int_A \nabla \mathbf{N}^{\mathrm{T}} \cdot \mathbf{g}^{\mathrm{T}} \, dA = \int_A \begin{bmatrix} \dfrac{\partial \mathbf{N}^{\mathrm{T}}}{\partial x} & \dfrac{\partial \mathbf{N}^{\mathrm{T}}}{\partial y} \end{bmatrix} \begin{bmatrix} y - y_{\mathrm{s}} \\ -x + x_{\mathrm{s}} \end{bmatrix} dA = \int_{-1}^{1}\int_{-1}^{1} \mathbf{B}^{\mathrm{T}} \begin{bmatrix} \mathbf{N}\mathbf{y} - y_{\mathrm{s}} \\ -\mathbf{N}\mathbf{x} + x_{\mathrm{s}} \end{bmatrix} |\mathbf{J}_{\mathrm{e}}| \, d\eta d\zeta . \tag{35}$$

The load vector which corresponds to Eq. (9) is

$$\mathbf{p}_{\mathrm{II}}^{\mathrm{e}} = -\int_A \left(\mathbf{N}^{\mathrm{T}} \cdot \mathbf{N}\right) \boldsymbol{\omega}_{\mathrm{I}}^{\mathrm{e}} \, dA = \int_{-1}^{1}\int_{-1}^{1} \left(\mathbf{N}^{\mathrm{T}} \cdot \mathbf{N}\right) \boldsymbol{\omega}_{\mathrm{I}}^{\mathrm{e}} |\mathbf{J}_{\mathrm{e}}| \, d\eta d\zeta . \tag{36}$$

On the basis of Eq. (36), to solve Eq. (9), first, one has to solve Eq. (8) to obtain the primary warping function. When the stiffness matrices and the load vectors of each element are combined into a global stiffness matrix and a global load vector, general solutions are obtained by solving linear systems of equations

$$\mathbf{K}\,\boldsymbol{\omega}_{\mathrm{I}} = \mathbf{P}_{\mathrm{I}} , \quad \mathbf{K}\,\boldsymbol{\omega}_{\mathrm{II}} = \mathbf{P}_{\mathrm{II}} . \tag{37}$$

After calculating the warping functions, the torsional constant and the warping moment of inertia are calculated from Eqs. (14) and (12) or (15), respectively. The angle of twist is calculated analytically from Eq. (18), in which, by setting the boundary conditions depending on the type of the beam supports, unknown constants ($C_1 \ldots C_4$) are determined. From there, it is easy to calculate the stresses by using Eqs. (4) and (5).

4. Numerical Examples

On the basis of the proposed finite element procedure, a computer program for stress analysis is developed. The accuracy of the presented model is illustrated by two examples. Stresses calculated by the computer program are the axial stress σ_z and the resultant shear stress τ, which is given as

$$\tau = \sqrt{{\tau_{zx}}^2 + {\tau_{zy}}^2} . \tag{38}$$

From Eq. (38), one should note that the resultant shear stress τ will always be positive since it only represents the intensity of the stress and not the direction.

Example 4.1 Figure 1 shows a symmetric I-beam fixed at both ends. The rotation about the z-axis is fully restrained while the warping is completely free. The beam is loaded by uniformly distributed torque m_z = 1 kNm/m. The elastic moduli are E = 210 GPa and G = 80.77 GPa. Since the cross-section is symmetric, the shear centre coincides with the centroid of the cross-section.

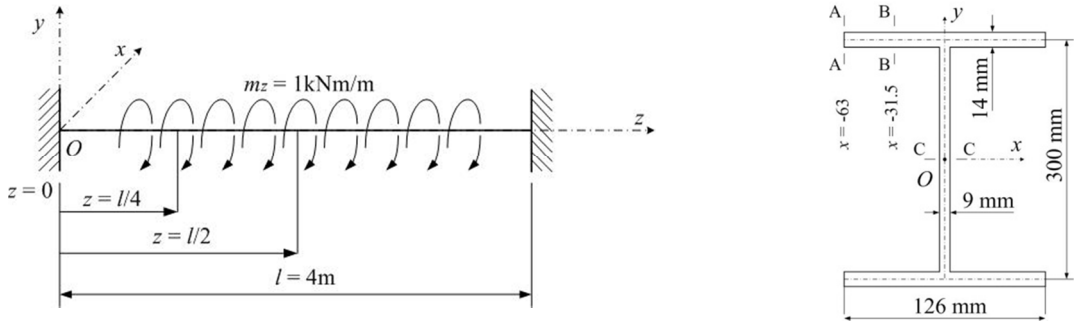

Fig. 1 Symmetric I-beam fixed at both ends

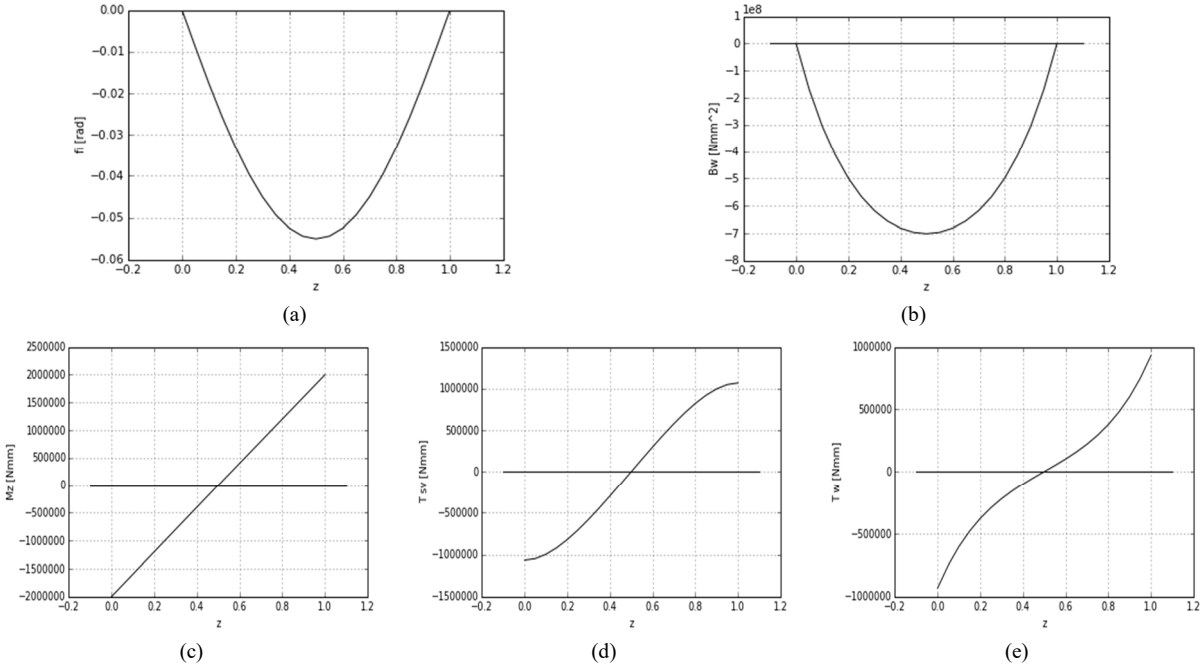

Fig. 2 Distribution of (a) the angle of twist φ, (b) of the bimoment B_ω, (c) of the torsional moment M_z, (d) St. Venant's moment T_{sv}, (e) the restrained warping moment T_ω over the length of the I-beam

Distributions of the angle of twist φ, bimoment B_ω, torsional moment M_z and its components over the length of the beam are shown in Figure 2. Since the intensity of the resultant shear stress τ is only calculated and since there is symmetry, it is enough to observe the beam from $z = 0$ to $z = l/2$.

The highest level of the axial stress in the cross-section occurs at $z = l/2$ since the bimoment value is highest there. Shear stress has its minimum/maximum at $z = 0$ and $z = l$. Distributions of the highest axial and shear stresses, by its components, are shown in Figure 3.

The cross-section is discretized by 1756 elements. The graphs above the flanges in Figure 3 (a) and (b) show the distribution of the described stress over the centre line of the flange. In Figure 3 (c), the graph above the flange and the graph on the right show the distribution of primary shear stress over the upper contour of the flange and over the right contour of the web, respectively. Since the corners of the cross-section are sharp, one can notice the appearance of very high stress concentrations on the graph on the right in Figure 3 (c). By filleting or chamfering the corners, such stress concentrations can be significantly reduced.

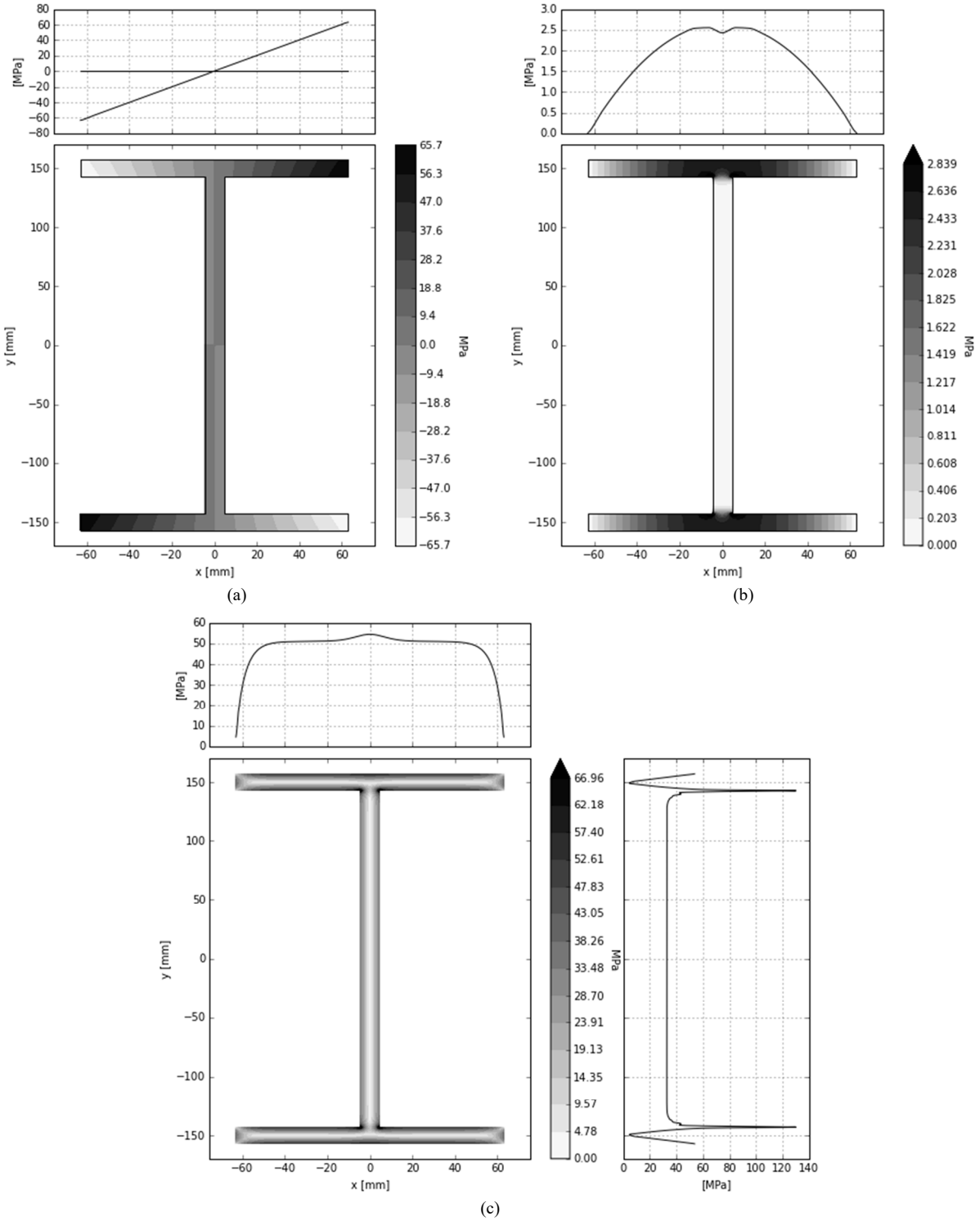

Fig. 3 Distribution of (a) the axial stress σ_z at $z = l/2$, (b) the secondary shear stress τ^{ω} at $z = 0$, (c) the primary shear stress τ^{sv} at $z = 0$ over the surface of the I-beam cross-section

This example was solved analytically by Šimić [17]. The numerical solution is compared with the analytical solution at three different cross-sectional cuts, for three different cross-section positions (marked in Figure 1). The compared values are shown in Tables 1, 2, and 3, where the values of the axial stress and of the secondary shear stress (σ_z, τ^{ω}) are shown for the centre line of the cross-sectional cut, while the values of the primary shear stress (τ^{sv}) are shown for one of the contours of the cross-sectional cut.

Table 1 Comparison between the numerical and analytical values of the axial stress σ_z on various cuts of the I-beam

		Numerical (MPa)	Analytical (MPa)
A – A	*z = 0*	0.00	0.00
A – A	*z = l/4*	– 50.93	– 50.12
A – A	*z = l/2*	– 63.14	– 62.00

Table 2 Comparison between the numerical and analytical values of the secondary shear stress τ^{ω} on various cuts of the I-beam

		Numerical (MPa)	Analytical (MPa)
B – B	*z = 0*	1.99	1.97
B – B	*z = l/4*	0.63	0.61
B – B	*z = l/2*	0.00	0.00

Table 3 Comparison between the numerical and analytical values of the primary shear stress τ^{sv} on various cuts of the I-beam

		Numerical (MPa)	Analytical (MPa)
B – B	*z = 0*	50.96	49.60
C – C		32.78	31.89
B – B	*z = l/4*	33.75	32.81
C – C		21.71	21.10
B – B	*z = l/2*	0.00	0.00
C – C		0.00	0.00

Example 4.2 Figure 4 shows a cantilevered U-beam loaded with the torsional moment M_z = 20 Nm at the free end. The elastic moduli are E = 210 GPa and G = 80.77 GPa.

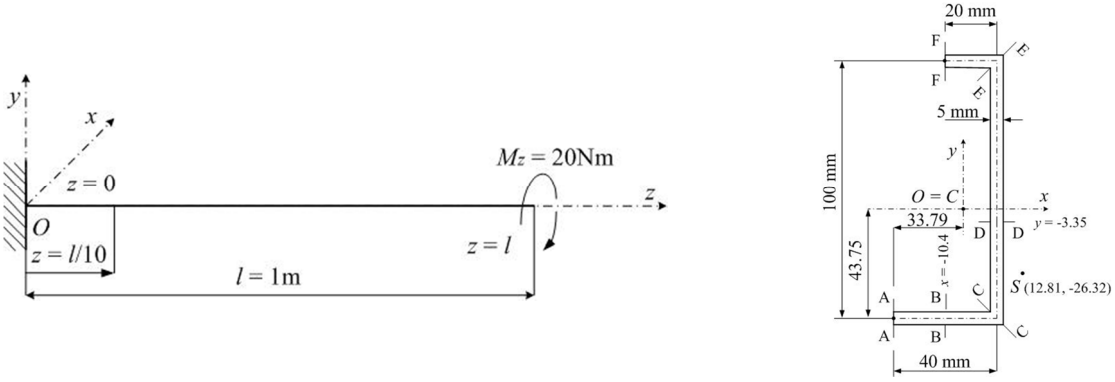

Fig. 4 Cantilevered U-beam

Distributions of the angle of twist φ, bimoment B_{ω}, torsional moment M_z and its components over the length of the beam are shown in Figure 5.

The highest level of axial stress occurs in the cross-section with the highest value of the applied bimoment, and that is in the cross-section at $z = 0$. The secondary shear stress has its maximum in the same cross-section, i.e. at $z = 0$. The highest level of primary shear stress occurs in the cross-section at $z = l$. Distributions of the highest axial and the highest shear stress, by its components, are shown in Figure 6.

The cross-section is discretized by 1884 elements. The graphs in Figure 6 (a) and (b) show the distributions of the described stress over the centre line of the U profile while those in Figure 6 (c) show the distributions of the primary shear stress over the outer contour of the U profile.

A similar example is solved analytically by Chen and Atsuta [2]. The numerical solution is compared to the analytical one at six different cross-sectional cuts, for three different cross-section positions (marked in Figure 4). The compared values are shown in Tables 4, 5, and 6, where the values of the axial stress and of the secondary shear stress (σ_z, τ^{ω}) are shown for the centre line of the cross-sectional cut, while the values of the primary shear stress (τ^{sv}) are shown for one of the contours of the cross-sectional cut.

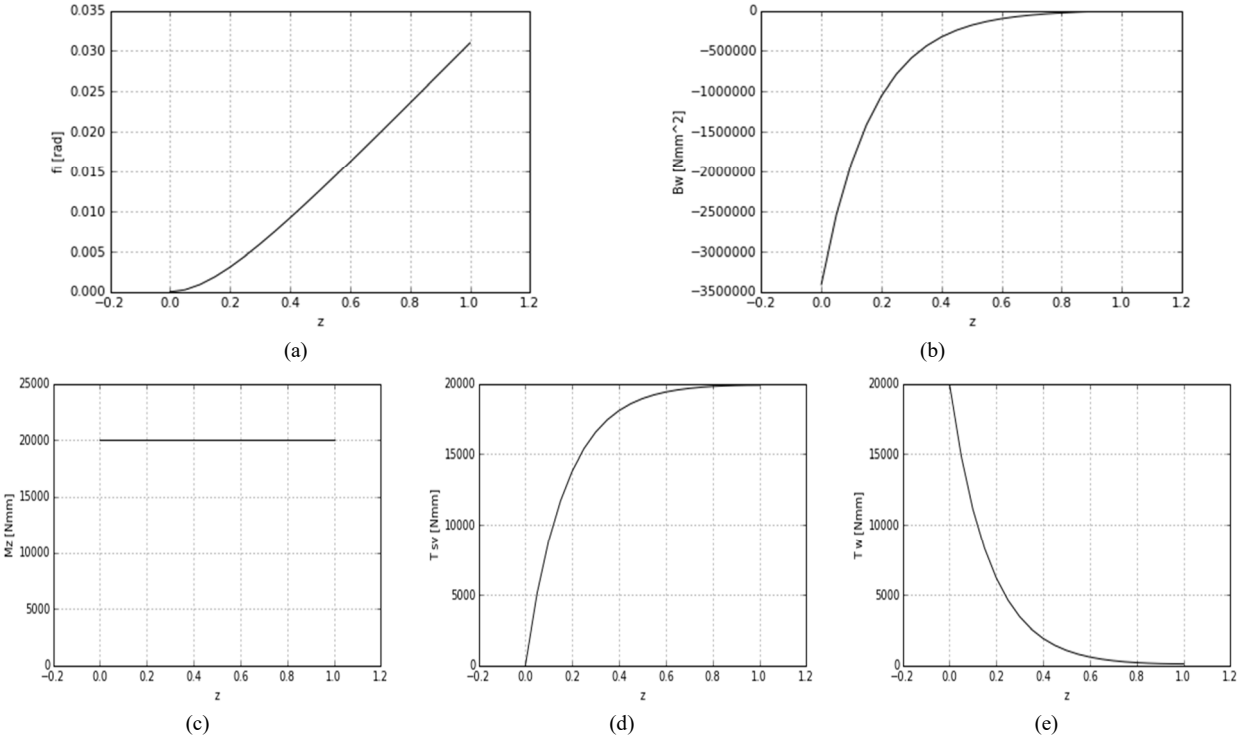

Fig. 5 Distribution of (a) the angle of twist φ , (b) the bimoment B_ω (c) the torsional moment M_z , (d) St. Venant's moment T_{sv} , (e) the restrained warping moment T_ω over the length of the U-beam

Table 4 Comparison between the numerical and analytical values of the axial stress σ_z on various cuts of the U-beam

		Numerical (MPa)	Analytical (MPa)
A – A	*z = 0*	19.27	18.07
C – C		– 12.71	– 12.82
E – E		17.94	18.87
F – F		– 57.96	– 59.58
A – A	*z = l/10*	10.72	9.92
C – C		– 7.07	– 7.03
E – E		9.98	10.36
F – F		– 32.23	– 32.70
A – A	*z = l*	0.00	0.00
C – C			
E – E			
F – F			

Table 5 Comparison between the numerical and analytical values of the primary shear stress τ^{sv} on various cuts of the U-beam

		Numerical (MPa)	Analytical (MPa)
B – B	*z = 0*	0.00	0.00
D – D			
B – B	*z = l/10*	6.70	6.79
D – D		6.70	6.79
B – B	*z = l*	15.00	14.97
D – D		15.00	14.97

Table 6 Comparison between the numerical and analytical values of the secondary shear stress τ^{ω} on various cuts of the U-beam

		Numerical (MPa)	Analytical (MPa)
B – B	*z = 0*	1.36	1.27
D – D		– 0.80	– 0.92
B – B	*z = l/10*	0.75	0.70
D – D		– 0.44	– 0.51
B – B	*z = l*	0.01	0.01
D – D		– 0.01	– 0.01

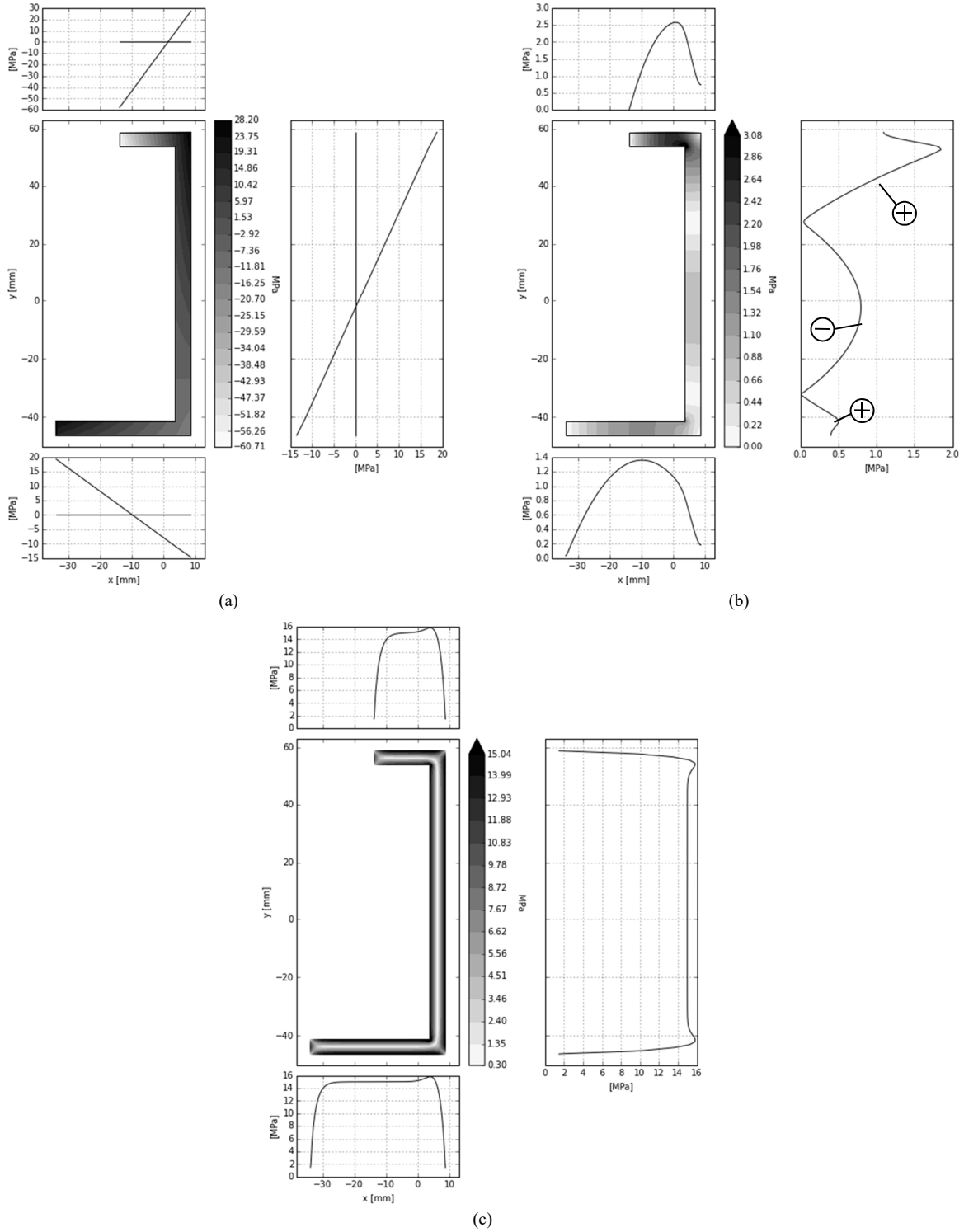

Fig. 6 Distribution of (a) the axial stress σ_z at $z = 0$ (b) the secondary shear stress τ^{ω} at $z = 0$ (c) Distribution of the primary shear stress τ^{SV} at $z = l$ over the surface of the U-beam cross-section

5. Conclusions

This paper has presented a model for the elastic stress analysis of beams under non-uniform torsion. A genuine solution has been reached using the finite element method. The reliability of the proposed numerical model has been verified by studying two examples which showed a certain degree of accuracy. Due to stress concentrations, the solution proposed in this paper slightly differs from the analytical solution, but the difference can be reduced by

applying fillets or chamfers on the corners of the cross-section. This solution is able to display stress distributions over the surface of the cross-section. Future research will extend the proposed algorithm to a model with the material and geometric nonlinearity. For that purpose, the angle of twist will be solved numerically. Since the model is able to show stress distribution, the idea is to display gradual plastification over the surface of the cross-section.

Acknowledgement

The authors gratefully acknowledge the financial support of the Croatian Science Foundation (project No. 6876) and the University of Rijeka (13.09.1.1.03).

REFERENCES

[1] W. D. Pilkey: Analysis and Design of Elastic Beams, Computational Methods. John Wiley & Sons, New York 2002. DOI: 10.1002/9780470172667

[2] W. F. Chen, T. Atsuta: Theory of Beam-Columns, Volume 2: Space behavior and design. J. Ross Publishing, Fort Lauderdale, FL 2008.

[3] J. J. Connor: Analysis of Structural Member Systems. Ronald Press, 1976.

[4] S. Timoshenko, J. Goodier: Theory of Elasticity. McGraw-Hill Co., NY, 1970.

[5] V. Z. Vlasov: Thin-Walled Elastic Bars (in Russian). 2nd ed., Fizmatgiz, Moscow, 1959.

[6] Gjelsvik: The Theory of Thin Walled Bars. John Wiley & Sons, New York 1981.

[7] J. Brnić, G. Turkalj, M. Čanađija: Shear stress analysis in engineering beams using deplanation field of special 2-D finite elements. Meccanica, vol. 45 (2010), pp 227-235. DOI: 10.1007/s11012-009-9241-z

[8] Stefan, M. Lupoae, D. Constantin, C. Baciu: Numerical Determinations with Finite Differences Method of Prismatic Beams Subjected to Torsion. Proceedings of the World Congress on Engineering 2012 Vol III, WCE 2012, London, U.K.

[9] E. J. Sapountzakis: Bars under Torsional Loading: A Generalized Beam Theory Approach. ISRN Civil Engineering, vol. 2013, Article ID 916581, 39 pages, 2013. DOI: 10.1155/2013/916581

[10] R. E. Fatmi: Non-uniform warping including the effects of torsion and shear forces. Part I: A general beam theory. International Journal of Solids and Structures, vol. 44 (2007), pp 5912-5929. DOI: 10.1016/j.ijsolstr.2007.02.006

[11] R. E. Fatmi: Non-uniform warping including the effects of torsion and shear forces. Part II: Analytical and numerical applications. International Journal of Solids and Structures, vol. 44 (2007), pp 5930-5952. DOI: 10.1016/j.ijsolstr.2007.02.005

[12] E. J. Sapountzakis, V. G. Mokos: Warping shear stresses in nonuniform torsion by BEM. Computaional Mechanics, vol. 30 (2003), pp 131-142. DOI: 10.1007/s00466-002-0373-4

[13] E. J. Sapountzakis, V. G. Mokos: Dynamic analysis of 3-D beam elements including warping and shear deformation effects. International Journal of Solids and Structures, vol. 43 (2006), pp 6707-6726. DOI: 10.1016/j.ijsolstr.2006.02.004

[14] Chang-New Chen: The warping torsion bar model of the differential quadrature element method. Computers and Structures, vol. 66, Issues 2-3 (1998), pp 249-257

[15] Z. Wang, J. Zhao, D. Zhang, J Gong: Restrained torsion of open thin-walled beams including shear deformation effects. Journal Zhejiang Univ-Sci A (Appl Phys & Eng), vol. 13, Issue 4 (2012), pp 260-273

[16] G. Turkalj, J. Brnić: Nonlinear Stability Analysis of Thin-walled Frames Using UL-ESA Formulation. International Journal of Structural Stability and Dynamics, vol. 4, No. 1 (2004), pp 45-67. DOI: 10.1142/S0219455404001094

[17] V. Šimić: Otpornost Materijala II. Školska knjiga, Zagreb 1995.

Submitted: 29.01.2016

Accepted: 10.5.2016

Associate expert Damjan Banić
Prof. dr. sc. Goran Turkalj
Prof. dr. sc. Josip Brnić
University of Rijeka
Faculty of Engineering
Department of Engineering Mechanics
Vukovarska 58
51000 Rijeka Croatia